AIAA 2002-0891

A Phase-Field Model of Convection With Solidification

D.M. Anderson
George Mason University
Fairfax, VA

G.B. McFadden
National Institute of Standards and Technology
Gaithersburg, MD

A.A. Wheeler
University of Southampton
Southampton, UK

40th AIAA Aerospace Sciences Meeting & Exhibit
14-17 January 2002 / Reno, NV

AIAA 2002-0891

A PHASE-FIELD MODEL OF CONVECTION WITH SOLIDIFICATION

D.M. Anderson
Department of Mathematical Sciences
George Mason University
Fairfax, VA 22030, USA

G.B. McFadden
Mathematical and Computational Sciences Division
National Institute of Standards and Technology
Gaithersburg, MD 20899-8910, USA

A.A. Wheeler
Faculty of Mathematical Studies
University of Southampton
Highfield, Southampton, SO17 1BJ, UK

October 30, 2001

ABSTRACT

A phase-field model for the solidification of a pure material that incorporates convection has recently been developed [Anderson, McFadden and Wheeler, Physica D, 135 (2000) pp. 175–194]. This model is a two-fluid model in which the solid phase is modeled as a sufficiently viscous fluid. The model allows for the solid and liquid phases to have different densities and hence allows for expansion or contraction flows upon solidification. In this paper we investigate numerically a simplified version of this model by considering solidification occurring between the two closely-spaced parallel plates of a Hele-Shaw cell. We assess two key aspects of the model: (1) the effect of density differences between the solid and liquid phases during dendritic growth and (2) the role played by the viscosity ratio between the solid and liquid phases.

INTRODUCTION

In order to model the solidification of a pure fluid, one must generally accomplish at least two things simultaneously: (i) determine the thermal field in the bulk solid and liquid phases and (ii) determine the position of the interface between these solid and liquid phases. The classical approach to this problem takes the point of view that the interface separating the bulk phases is a mathematical boundary of zero thickness where interfacial conditions are applied. These interfacial conditions couple to the thermal transport equations in the bulk and this system of equations and boundary conditions provides a means to address (i) and (ii). In a phase-field model for the solidification of a pure fluid, a phase-field variable ϕ which varies in space and time is introduced to characterize the phase of the material. In place of the "sharp" transition from solid to liquid phases that characterizes the classical approach, here the phase-field varies smoothly but rapidly through an interfacial region. Additionally, in place of the interfacial jump conditions used in the classical description a partial differential equation applied over the entire computational domain governs the evolution of ϕ. The effect is a formulation of the free boundary problem that does not require the explicit application of interfacial conditions at the unknown location of a phase boundary. A number of closely related formulations of phase-field models of a pure material exist[1,2,3] including derivations[4,5] based on the formalism of irreversible thermodynamics[6].

The above description requires further modification if hydrodynamic effects such as buoyancy-driven convection, externally forced flows or density-change driven flows are present during solidification. Such hydrodynamic effects on dendritic growth have been observed experimentally by Glicksmann et al[7,8,9] and can manifest themselves in complex ways, including the preferential sidebranching on one side of a grow-

ing dendrite depending on flow characteristics. Early efforts to include the effects of fluid flow in phase-field models have been given by Caginalp and Jones[10,11]. Using ideas developed in the context of diffuse interface models of hydrodynamics[12,13], Anderson, McFadden and Wheeler derived[14] and analyzed[15,16] a phase-field model for the solidification of a pure material that includes the effects of fluid flow. Other work in this area includes that by Beckermann, Karma and coworkers[17,18,19,20] and Tönhardt and Amberg[21,22,23,24]. Related approaches that use front tracking methods[25,26] are also underway.

In the present paper we solve numerically a simplified version of the model derived in Anderson, McFadden and Wheeler[14] using a general purpose adaptive finite difference algorithm (VLUGR)[27]. These calculations directly extend the work by Braun et al.[28,29], who calculated dendritic growth of a pure material into an undercooled melt phase without fluid flow. Earlier calculations on a model closely related to the one used here have also been performed.[30]

GOVERNING EQUATIONS

We take as our starting point the anisotropic form of the dimensionless equations given in Anderson, McFadden and Wheeler[16]. These equations are based on a formulation that includes gradient and double well terms with respect to the energy but not with respect to the entropy. These equations are

$$\frac{\partial \rho}{\partial t} + \nabla \cdot (\rho \vec{u}) = 0, \tag{1a}$$

$$\rho \frac{D\vec{u}}{Dt} = \nabla \cdot \Bigg\{ -pI + Pr\tau + \tilde{\gamma}\epsilon \left[\frac{1}{2}\Gamma^2(\nabla\phi) I - \Gamma(\nabla\phi)\vec{\xi} \otimes \nabla\phi \right] \Bigg\}, \tag{1b}$$

$$\epsilon^2 \tau \frac{D\phi}{Dt} = \epsilon^2 \nabla \cdot \left[\Gamma(\nabla\phi)\vec{\xi} \right] - \rho \left[\lambda T r'(\phi) + \frac{1}{2} H_m'(\phi) + \frac{\epsilon}{\tilde{\gamma}} p \frac{\partial}{\partial \phi}\left(\frac{1}{\rho}\right) \right], \tag{1c}$$

$$\rho \frac{D}{Dt}\left[T - r(\phi) + \frac{\delta}{2} H_m(\phi) - \frac{\epsilon S p^*}{\lambda \tilde{\gamma}} \frac{1}{\rho} \right] = \nabla \cdot [Q(\phi)\nabla T] + \epsilon^2 \nu \nabla \cdot \left[\Gamma(\nabla\phi)\vec{\xi} \right] \frac{D\phi}{Dt} + \frac{\epsilon S}{\lambda \tilde{\gamma}} [-(p+p^*)I + Pr\tau] : \nabla \vec{u}. \tag{1d}$$

Here ρ is the fluid density assumed to be a function of the phase field ϕ [see equation (8a)], $\vec{u}$ is the fluid velocity, p is the pressure, T is the temperature and $\tau = \mu(\phi)[\nabla\vec{u} + (\nabla\vec{u})^T - \frac{2}{3}(\nabla\cdot\vec{u})I]$ is the viscous stress tensor, where $\mu(\phi)$ is the viscosity assumed to be a function ϕ [see equation (8b)]. Anisotropy is incorporated through the generalized ξ–vector $\vec{\xi}$ and the anisotropic surface energy function $\Gamma(\phi)$.[31,32,16] Here $Pr = \nu_L/\kappa_L$ is the Prandtl number which relates the kinematic viscosity in the liquid to the thermal diffusivity in the liquid, $\tilde{\gamma}$ is a dimensionless measure of the surface energy, ϵ is a dimensionless interface thickness, τ is an interface mobility parameter, λ is a latent heat parameter which can also be interpreted as the ratio between interface thickness and capillary length scales, δ is a double-well parameter associated with the internal energy, $S = L/cT_M$ is a Stefan number where L is the latent heat per unit mass and c is the heat capacity per unit mass, and p^* is a dimensionless reference pressure. The function $Q(\phi)$ represents the thermal conductivity in the material. The functions $r(\phi)$ and $H_m(\phi)$ are defined in the text after equation (8). We refer the reader to Anderson, McFadden and Wheeler[16] for more details regarding these equations.

We further simplify the above model by making the following approximations and assumptions. First, we consider only the case of equal thermal conductivities in the solid and liquid phases so that $Q(\phi) = 1$. Second, we neglect the classical and non-classical dissipation terms in the energy equation (1d). Third, we consider $\delta = 0$, which removes the double-well function in the energy equation. Fourth, we neglect the pressure effects associated with p^* and p in the energy and phase-field equations. The result of these assumptions is the following reduced set of equations

$$\frac{\partial \rho}{\partial t} + \nabla \cdot (\rho \vec{u}) = 0, \tag{2a}$$

$$\rho \frac{D\vec{u}}{Dt} = \nabla \cdot \Bigg\{ -pI + Pr\tau + \tilde{\gamma}\epsilon \left[\frac{1}{2}\Gamma^2(\nabla\phi) I - \Gamma(\nabla\phi)\vec{\xi} \otimes \nabla\phi \right] \Bigg\}, \tag{2b}$$

$$\epsilon^2 \tau \frac{D\phi}{Dt} = \epsilon^2 \nabla \cdot \left[\Gamma(\nabla\phi)\vec{\xi} \right] - \rho \left[\lambda T r'(\phi) + \frac{1}{2} H_m'(\phi) \right], \tag{2c}$$

$$\rho \frac{D}{Dt}[T - r(\phi)] = \nabla^2 T. \tag{2d}$$

As a final simplification of the above model we shall examine the equations in a Hele-Shaw geometry so that the length scale associated with the narrow gap in the z direction is much smaller than the in-plane length scales associated with the x and y directions. We take the ratio of gap thickness to in-plane length scale to be $\delta_H \ll 1$.

We define $Z = z/\delta_H$ so that $\partial/\partial z = (\partial/\partial Z)/\delta_H$,

expand the independent variables in powers of δ_H and consider the limit $\delta_H \to 0$ with all other parameters held fixed. Specifically, we take

$$\phi = \phi_0 + \delta_H \phi_1 + \delta_H^2 \phi_2 + \ldots, \quad (3a)$$

$$T = T_0 + \delta_H T_1 + \delta_H^2 T_2 + \ldots, \quad (3b)$$

$$p = \frac{1}{\delta_H^2}\left[p_0 + \delta_H p_1 + \ldots\right], \quad (3c)$$

$$w = w_0 + \delta_H w_1 + \delta_H^2 w_2 + \ldots, \quad (3d)$$

$$\vec{u}_\perp = \vec{u}_\perp^{(0)} + \delta_H \vec{u}_\perp^{(1)} + \ldots, \quad (3e)$$

where $\vec{u} = (\vec{u}_\perp, w) = (u, v, w)$. Note that the pressure must be rescaled to balance the viscous terms in the momentum equation.

The leading order equations show that ϕ_0, T_0 and p_0 are independent of Z and that the leading-order vertical flow w_0 vanishes. The in-plane velocity is

$$\vec{u}_\perp^{(0)} = -\frac{1}{2Pr}\frac{\nabla_\perp p_0}{\mu(\phi_0)}\left(Z^2 - Z\right). \quad (4)$$

Consequently, the vertically-averaged flow is driven by horizontal pressure gradients

$$\langle \vec{u}_\perp^{(0)} \rangle = -\frac{1}{12Pr}\frac{\nabla_\perp p_0}{\mu(\phi_0)}. \quad (5)$$

Note that the capillary term in the momentum equation does not contribute at this order. Equations for the leading-order quantities can be obtained through averaging of the phase-field equation, energy equation and continuity equation, respectively. We introduce a rescaled temperature $\theta_0 = T_0/S_\infty$ where $S_\infty = c(T_M - T_\infty)/L$ is the degree of undercooling in the liquid, T_∞ is a dimensional far-field temperature and T_M is the equilibrium melting temperature of the material. This leads to our computational model

$$\epsilon^2 \tau\left[\frac{\partial \phi_0}{\partial t} - \frac{1}{12Pr}\frac{1}{\mu(\phi_0)}\nabla_\perp \phi_0 \cdot \nabla_\perp p_0\right] =$$

$$\epsilon^2 \nabla_\perp \cdot \Gamma_{\perp 0} - \rho(\phi_0)\left[\lambda S_\infty \theta_0 r'(\phi_0) + \frac{1}{2}H_m'(\phi_0)\right], \quad (6a)$$

$$\rho(\phi_0)\left[\frac{\partial \theta_0}{\partial t} - \frac{1}{S_\infty}r'(\phi_0)\frac{\partial \phi_0}{\partial t} - \frac{1}{12Pr}\frac{1}{\mu(\phi_0)} \times \right.$$

$$\left. \nabla_\perp p_0 \cdot \left(\nabla_\perp \theta_0 - \frac{1}{S_\infty}r'(\phi_0)\nabla_\perp \phi_0\right)\right] = \nabla_\perp^2 \theta_0, \quad (6b)$$

$$\nabla_\perp^2 p_0 = 12Pr\frac{\rho'(\phi_0)\mu(\phi_0)}{\rho(\phi_0)}\frac{\partial \phi_0}{\partial t}$$

$$+\frac{\rho(\phi_0)\mu'(\phi_0) - \mu(\phi_0)\rho'(\phi_0)}{\rho(\phi_0)\mu(\phi_0)}\nabla_\perp \phi_0 \cdot \nabla_\perp p_0, \quad (6c)$$

which is a set of three equations for the phase field variable, temperature and pressure.

Anisotropy enters this simplified model through the phase-field equation only. We shall follow Braun and Murray[28] and use four-fold anisotropy via the function $\Gamma(\nabla\phi) = |\nabla\phi|(1 + b\cos 4\beta)$ where $\tan\beta = \phi_y/\phi_x$ and b is a constant parameter with $0 < b < \frac{1}{15}$. The anisotropic term in the phase-field equation is

$$\nabla_\perp \cdot \Gamma_{\perp 0} = \frac{\partial}{\partial x}\left\{\left[1 + b\cos 4\beta_0\right] \times \right.$$

$$\left.\left[\phi_{0x}\left(1 + b\cos 4\beta_0\right) + \phi_{0y} 4b \sin 4\beta_0\right]\right\}$$

$$+\frac{\partial}{\partial y}\left\{\left[1 + b\cos 4\beta_0\right] \times \right.$$

$$\left.\left[\phi_{0y}\left(1 + b\cos 4\beta_0\right) - \phi_{0x} 4b \sin 4\beta_0\right]\right\}, \quad (7)$$

where $\tan\beta_0 = \phi_{0y}/\phi_{0x}$.

The density and viscosity functions are taken to have the form

$$\rho(\phi) = 1 + (\rho_S/\rho_L - 1)r(\phi), \quad (8a)$$

$$\mu(\phi) = 1 + (\mu_S/\mu_L - 1)r(\phi), \quad (8b)$$

where the interpolation function has the form $r(\phi) = \phi^3(10 - 15\phi + 6\phi^2)$. Finally, we define the double-well function $H_m(\phi)$ by $\rho(\phi)H_m(\phi) = \frac{1}{2}\phi^2(1-\phi)^2$. In the absence of fluid flow where $\rho(\phi) = \mu(\phi) = 1$, this model reduces to that of Braun and Murray[28]. A closely related model has been examined previously[30] for the case of viscosity ratio $\mu_S/\mu_L = 1$.

NUMERICAL COMPUTATIONS

In the calculations, the computational domain is a rectangular box of dimensions X_0 and Y_0 in the x and y directions, respectively. We consider three different sets of boundary conditions applied at these boundaries corresponding to cases (i), (ii) and (iii) described in the caption of Table 1. In cases (i) and (ii) there is no externally-forced flow, only flows due to contraction or expansion upon solidification are present. In case (iii) we impose via a pressure difference a uniform flow from left to right in the computational domain. The initial conditions correspond to a spherical solid particle with a four-fold perturbation centered at (X_c, Y_c). The liquid phase ($\phi_0 = 0$) is initially undercooled $\theta_0 = -1$ and the solid phase ($\phi_0 = 1$) has a temperature of $\theta_0 = 0$. We follow Braun and Murray[28] and use 'smoothed' versions of these values as the initial conditions. Additionally, we initialize the pressure by setting $p_0 = 1$ everywhere. In cases (i) and (ii) we use $(X_c, Y_c) = (0, 0)$

	box (bc)	t	ρ_S/ρ_L	μ_S/μ_L	$1/Pr$
A	3x1 (i)	0.50	0.9	2	1.2
B	3x1 (i)	0.50	1.0	2	1.2
C	3x1 (i)	0.50	1.1	2	1.2
D	3x1 (ii)	0.50	0.9	2	1.2
E	3x1 (ii)	0.50	0.9	1	1.2
F	3x3 (i)	0.50	0.9	1	1.2
G	3x1 (iii)	0.02	1.0	5	1.2
H	3x1 (iii)	0.02	1.0	5	600
I	3x1 (iii)	0.02	1.0	5	1200
J	3x1 (iii)	0.02	1.0	5	2400
K	3x1 (iii)	0.02	1.0	80	2400
L	3x1 (iii)	0.02	1.0	160	2400
M	3x1 (iii)	0.02	1.0	320	2400

Table 1: In these calculations $\epsilon = 0.005$, $b = 0.015$, $\lambda = 0.5$, $1/\tau = 0.1$ and $S_\infty = 0.5$. The boundary conditions correspond to Neumann conditions on all external boundaries for ϕ_0, θ_0 and p_0 except (i): $p_0 = 1$ at the right and upper boundaries, (ii): $p_0 = 1$ at the right boundary, and (iii) $p_0 = 1$ at the right boundary and $p_0 = 0$ at the left boundary.

which takes advantage of the left/right and up/down symmetry of the growing dendrite. In case (iii) we use $(X_c, Y_c) = (\frac{1}{2}X_0, 0)$ where the imposed flow allows only up/down symmetry.

Dendrites with expansion or contraction flow:

In the first set of calculations we examine the effects of density change on the growth of a dendrite. The initial particle is centered at $(X_c, Y_c) = (0, 0)$ and has an average dimensionless radius of 0.1.

Figure 1 shows a dendrite with $\rho = 1.1$ (contraction flow) in the upper diagram and a dendrite with $\rho = 0.9$ (expansion flow) in the lower diagram (which has been reflected about the axis $y = 0$ to facilitate a comparison between the two cases). At this stage, the primary growth is associated with the tip growing in the x direction. There is a pressure minimum with $p \approx 0.1$ (maximum with $p \approx 1.8$) for the dendrite with $\rho = 1.1$ ($\rho = 0.9$) driving a flow towards (away from) the growing tip. These pressure extremes are in part due to the fixed pressure condition at $y = 1$ and the proximity of the dendrite to this wall. Figure 2 shows the position of this tip and its temperature as a function of time for these two calculations and also that for $\rho = 1$. We see that the dendrite corresponding to the expansion flow ($\rho < 1$) grows faster than its counterpart with contraction flow ($\rho > 1$). The increase in velocity with decreasing ρ is comparable to the increase in Peclet number [$Pe = RV/2\kappa$, where R is a tip radius, V is a tip velocity and κ is the thermal diffusivity] with decreasing ρ that was found in analytical results of dendritic growth with expansion or contraction flow obtained by McFadden and Coriell[33] (see their figure 4).

In figure 3 we show the growth of two dendrites (cases D and E) with $\rho = 0.9$ (expansion flow) for the boundary conditions in case (ii). The Neumann boundary conditions on both upper and lower boundaries may be more representative of a symmetric array of dendrites growing in the x direction than the dendrites in figure 1. In the upper diagram the viscosity ratio is $\mu = 2$ while the lower diagram shows the case $\mu = 1$. In each case we observe a compression of the pressure contours in the liquid in front of the tip and in contrast to the results in figure 1 do not observe a local pressure minimum or maximum. The dendrite with $\mu = 2$ (upper diagram) grows slightly slower than that for $\mu = 1$. In either case, there is very little fluid flow generated in the "solid" phase despite the low viscosity ratios. The pressure varies from a dimensionless value of unity in the far-field liquid ($x = 3$) to a value near 4 (when $\mu = 2$) and 3.5 (when $\mu = 1$) near $x = 0$.

In figure 4 a dendrite (case F) with $\rho = 0.9$ (expansion flow) is computed in a larger domain. One can observe the flow generated at each of the growing tips in a symmetric fashion unlike figure 1. The pressure varies from a dimensionless value of unity in the far-field liquid boundaries to a value near 2.2 inside the solid phase. There is a tendency for the flow far from the tip to be concentrated near the upper left and lower right regions of the domain and for a rather weak flow in the upper right region. This is a consequence of the fixed pressure boundary conditions which lead to a nearly uniform pressure in the upper right corner.

Dendrites in a uniform flow field:

Here we examine dendrites growing in the presence of a uniform flow field. The initial particle is centered at $(X_c, Y_c) = (1.5, 0)$ and has an average dimensionless radius of 0.1.

In figure 5 four cases (G–J in Table 1) are shown in which the growing dendrite experiences an imposed uniform flow from left to right. All parameters are held fixed in the four diagrams with the exception of $1/Pr$ which increases from a value of 1.2 (top) to 2400 (bottom). Recall that $Pr = \nu_L/\kappa$ is the ratio of kinematic viscosity to liquid thermal diffusivity. In our model, increasing $1/Pr$ effectively amplifies the effect of the velocity field. When $1/Pr = 1.2$ the dendrite grows nearly symmetrically in the horizontal direction (the corresponding thermal field, not shown, also appears nearly symmetric). However, as $1/Pr$ is

increased a distortion of the growing dendrite can be observed. This distortion is both a direct and indirect consequence of the flow. First, there is a direct effect on the shape of the solid through a hydrodynamic (viscous) distortion. This distortion is nonphysical for a true solid dendrite. Second, there is an indirect thermal effect on the growth of the particle due to a flow-induced nonuniformity of the thermal gradient surrounding the particle. For the case with $1/Pr = 2400$ translation, or advection, of the particle can also be observed. This sequence illustrates a limitation of the present two-fluid model to capture solid–body translation. A viscosity ratio of $\mu = 5$ for this particular flow configuration is not sufficient to maintain a solid-like dendrite. In figure 6 we show how these deficiencies can be overcome by increasing the viscosity ratio.

In figure 6 four cases (J–M in Table 1) are shown in which the growing dendrite again experiences an imposed uniform flow from left to right. Here all parameters, including Pr, are fixed except for the viscosity ratio, which is increased from $\mu = 5$ to $\mu = 320$ (top to bottom). A comparison shows that viscous distortion of the solid is eliminated as the viscosity ratio is increased. With a sufficiently large viscosity ratio the true growth asymmetry due to the flow can be observed. The thermal gradient in the liquid just to the left of the dendrite (upstream side) is amplified by the flow while that on the right (downstream side) is diminished; the consequence is an asymmetrically growing dendrite. Note that the increase of viscosity also eliminates the translation of the particle; this is consequence of the Hele-Shaw geometry in which the material (solid or liquid) must obey a no-slip condition on the confining plates. It is worth emphasizing that in the original model (before the Hele-Shaw geometry is considered) solid body motion is obtained as the viscosity ratio is increased[16].

With larger values of $1/Pr$ than those shown in figure 5 the particle can be completely swept away by the flow in the calculation. However, as demonstrated in Figure 6 using a sufficiently large viscosity ratio and the Hele-Shaw geometry in conjunction with a no-slip condition on the confining plates, the velocity in the solid approaches zero.

CONCLUSIONS

We have examined the effect of fluid flow on dendritic growth of a pure material into an undercooled melt using a two-fluid model in which the solid phase is modeled as a sufficiently viscous fluid. We have examined fluid flow generated by a volume change upon solidification and have observed the resulting expansion (contraction) flows when the solid is less (more) dense than the liquid. The pressure field associated with this flow generates relatively small fluid motion in the solid phase even for small viscosity ratios ($\mu_S/\mu_L = 1$ or 2). We have also examined the effect of a uniform flow past a growing dendrite. In this configuration, strong external flows can significantly distort the shape of the "solid" if the viscosity ratio is not taken sufficiently large. However, with the viscosity ratio sufficiently large, the solid phase can be successfully approximated by a viscous fluid. The Hele-Shaw approximation used in these calculations does not allow advection of solid particles attached to the confining plates and consequently no realistic advection of the dendrites was observed. However, the two-fluid model of the solid–liquid system is expected to allow solid–body motion in standard two or three dimensional calculations.

ACKNOWLEDGEMENTS

The authors would like to acknowledge support by the National Aeronautics and Space Administration Microgravity Science and Applications Program. We would like to thank R.J. Braun and B.T. Murray for providing us with a copy of their code into which we incorporated the fluid flow effects. The authors would also like to thank K. Brattkus for helpful conversations.

References

[1] G. Caginalp, in *Applications of Field Theory to Statistical Mechanics*, ed. L. Garrido, 216–226 Berlin: Springer-Verlag (1985).

[2] J.B. Collins and H. Levine, Phys. Rev. B **31** (1985) 6119.

[3] J.S. Langer, in *Directions in Condensed Matter Physics*, ed. G. Grinstein, G. Mazenko, 165–85. Philadelphia: World Scientific (1986).

[4] O. Penrose and P.C. Fife, Physica D **43** (1990) 44.

[5] S.-L. Wang, R.F. Sekerka, A.A. Wheeler, B.T. Murray, S.R. Coriell, R.J. Braun, and G.B. McFadden, Physica D **69** (1993) 189.

[6] S.R. de Groot and P. Mazur, *Non-Equilibrium Thermodynamics* (Dover, New York, 1984).

[7] S.C. Huang and M.E. Glicksman, Acta Metall. **29** (1981) 717.

[8] M.E. Glicksman and S.C. Huang, Convective heat transfer during dendritic growth, in *Convective Transport and Instability Phenomena*, ed. J. Zierep, H. Oertel Jr., 557–574 (Karlsruhe, G. Braun, 1982).

[9] M.E. Glicksman, S.R. Coriell, and G.B. McFadden, Ann. Rev. Fluid Mech. **18** (1986) 307.

[10] G. Caginalp and J. Jones, Appl. Math. Lett. **4** (1991) 97.

[11] G. Caginalp and J. Jones, in *On the Evolution of Phase Boundaries*, ed. M. E. Gurtin and G. B. McFadden, The IMA Series in Mathematics and Its Applications, Vol. 43 (Springer Verlag, New York, 1992) pp. 27–50.

[12] D. M. Anderson and G. B. McFadden, Phys. Fluids **9** (1997) 1870.

[13] D. M. Anderson, G. B. McFadden, and A. A. Wheeler, Ann. Rev. Fluid Mech. **30** (1998) 139.

[14] D. M. Anderson, G. B. McFadden and A. A. Wheeler, Physica D **135** (2000) 175.

[15] G. B. McFadden, A. A. Wheeler and D. M. Anderson, Physica D **144** (2000) 154.

[16] D. M. Anderson, G. B. McFadden and A. A. Wheeler, Physica D **151** (2001) 305.

[17] H. J. Diepers, C. Beckermann, and I. Steinbach, in *Solidification Processing 1997*, ed. J. Beech and H. Jones, Proc. 4th Decennial Int. Conf. on Solid. Process. (University of Sheffield, Sheffield, 1997) pp. 426–430.

[18] C. Beckermann, H.J. Diepers, I. Steinbach, A. Karma and X. Tong, J. Comp. Phys. **154** (1999) 468.

[19] X. Tong, C. Beckermann and A. Karma, Phys. Rev. E **61** (2000) R49.

[20] X. Tong, C. Beckermann, A. Karma and Q. Li, Phys. Rev. E **63** (2001) 1601.

[21] R. Tönhardt, Convective Effects on Dendritic Solidification, 1998 Ph. D. thesis, Department of Mechanics, Royal Institute of Technology, S-100 44 Stockholm, Sweden.

[22] R. Tönhardt and G. Amberg, J. Crystal Growth **194** (1998) 406.

[23] R. Tönhardt and G. Amberg, J. Crystal Growth **213** (2000) 161.

[24] R. Tönhardt and G. Amberg, Phys. Rev. E **62** (2000) 828.

[25] D. Juric and G. Tryggvason, J. Comp. Phys. **123** (1996) 127.

[26] G. Tryggvason, B. Bunner, A. Esmaeeli, D. Juric, N. Al-Rawahi, W. Tauber, J. Han, S. Nas and Y.J. Jan, J. Comp. Phys. **169** (2001) 708.

[27] J.G. Blom, R.A. Trompert and J.G. Verwer, ACM Trans. Math. Software **22** (1996) 302.

[28] R.J. Braun and B.T. Murray, J. Crystal Growth **174** (1997) 41.

[29] R.J. Braun, B.T. Murray and J. Soto Jr., Modelling Simul. Mater. Sci. Eng. **5** (1997) 365.

[30] D. M. Anderson, G. B. McFadden and A. A. Wheeler, A Phase-Field Model with Convection: Numerical Simulations, in *Interfaces for the Twenty-First Century*, ed. M.K. Smith et al. (Imperial College Press, London, 2001), to appear.

[31] A.A. Wheeler and G.B. McFadden, Eur. J. Appl. Math. **7** (1996) 367.

[32] A.A. Wheeler and G.B. McFadden, Proc. R. Soc. London A **453** (1997) 1611.

[33] G.B. McFadden and S.R. Coriell, J. Cryst. Growth **74** (1986) 507.

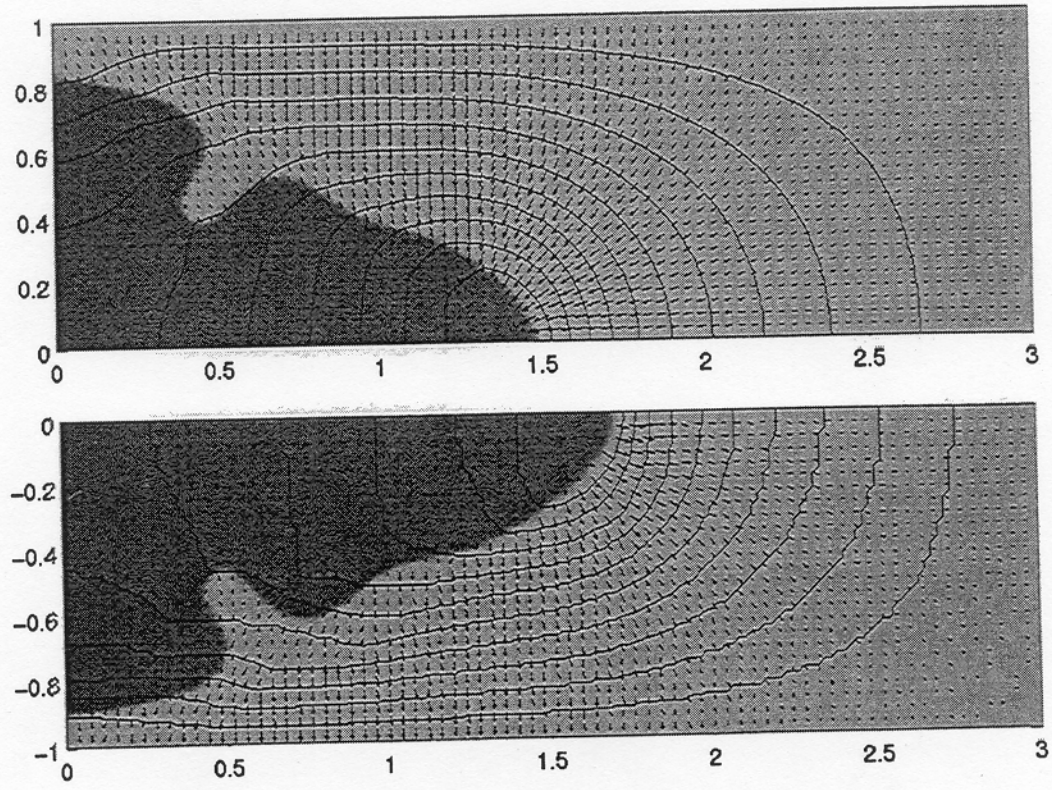

Figure 1: This figure shows dendritic growth into an undercooled liquid phase corresponding to case C (upper figure, $\rho = 1.1$) and case A (lower figure, $\rho = 0.9$). The phase-field is

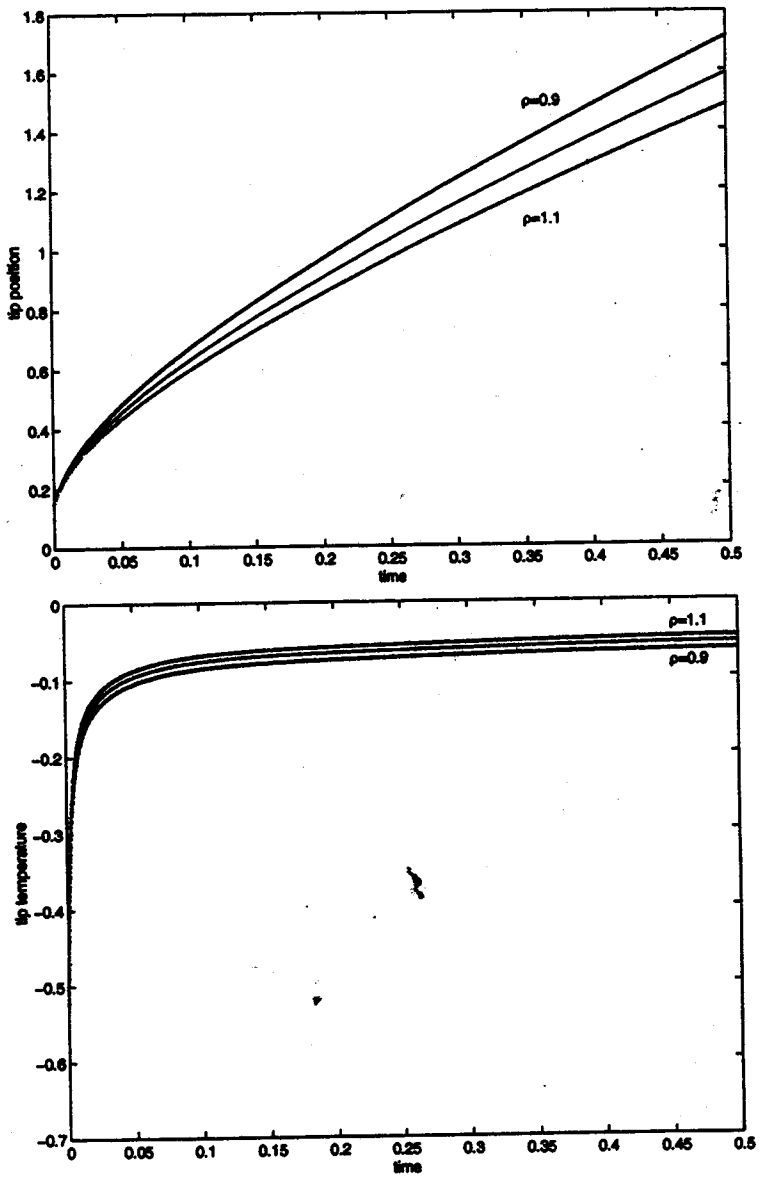

Figure 2: The tip position (in x direction) and tip temperature as a function of time for the dendrites in cases A, B and C. There is an expansion-type flow for the dendrite with $\rho = 0.9$ and a contraction-type flow for the dendrite with $\rho = 1.1$. The tip radius (not shown) is larger for the dendrite with $\rho = 0.9$ and smaller for the dendrite with $\rho = 1.1$.

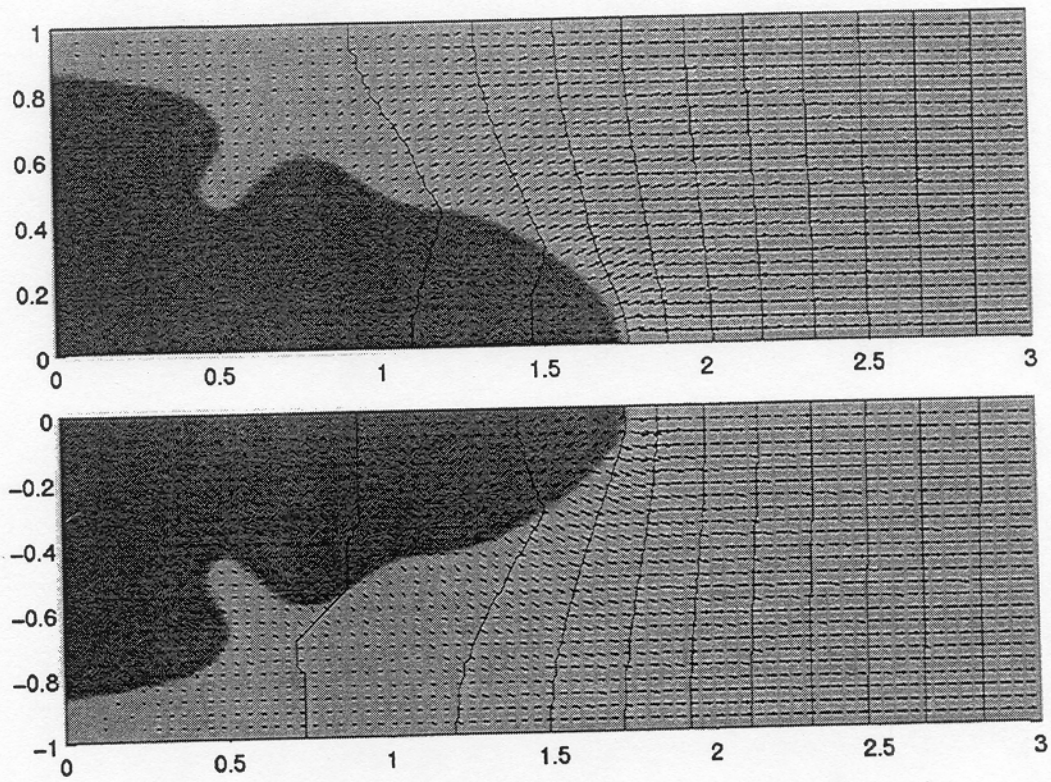

Figure 3: This figure shows the dendrites for cases D (upper) and E (lower).

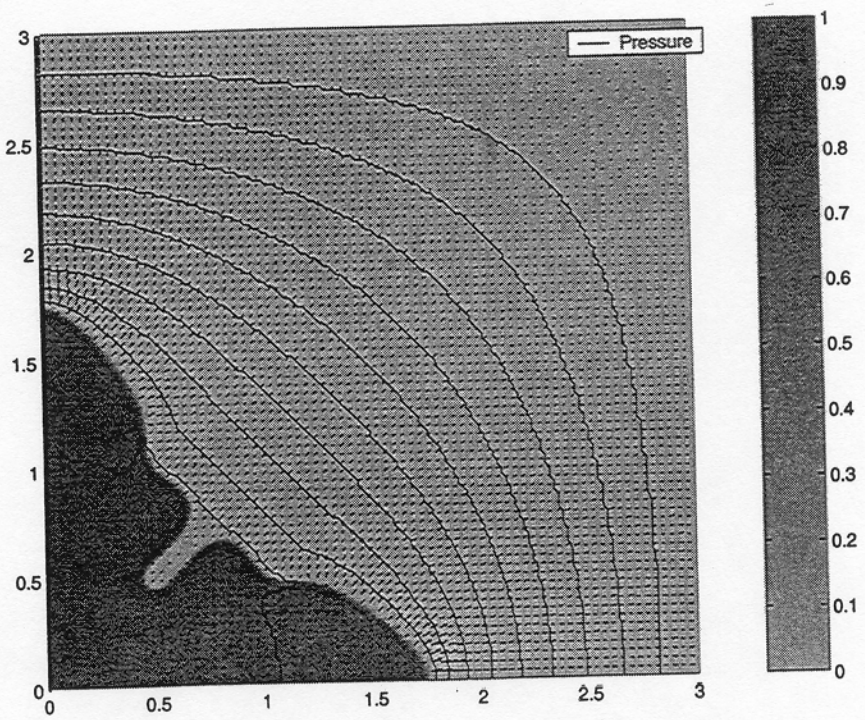

Figure 4: This figure shows the dendrite for case F. The colorbar indicates the value of ϕ.

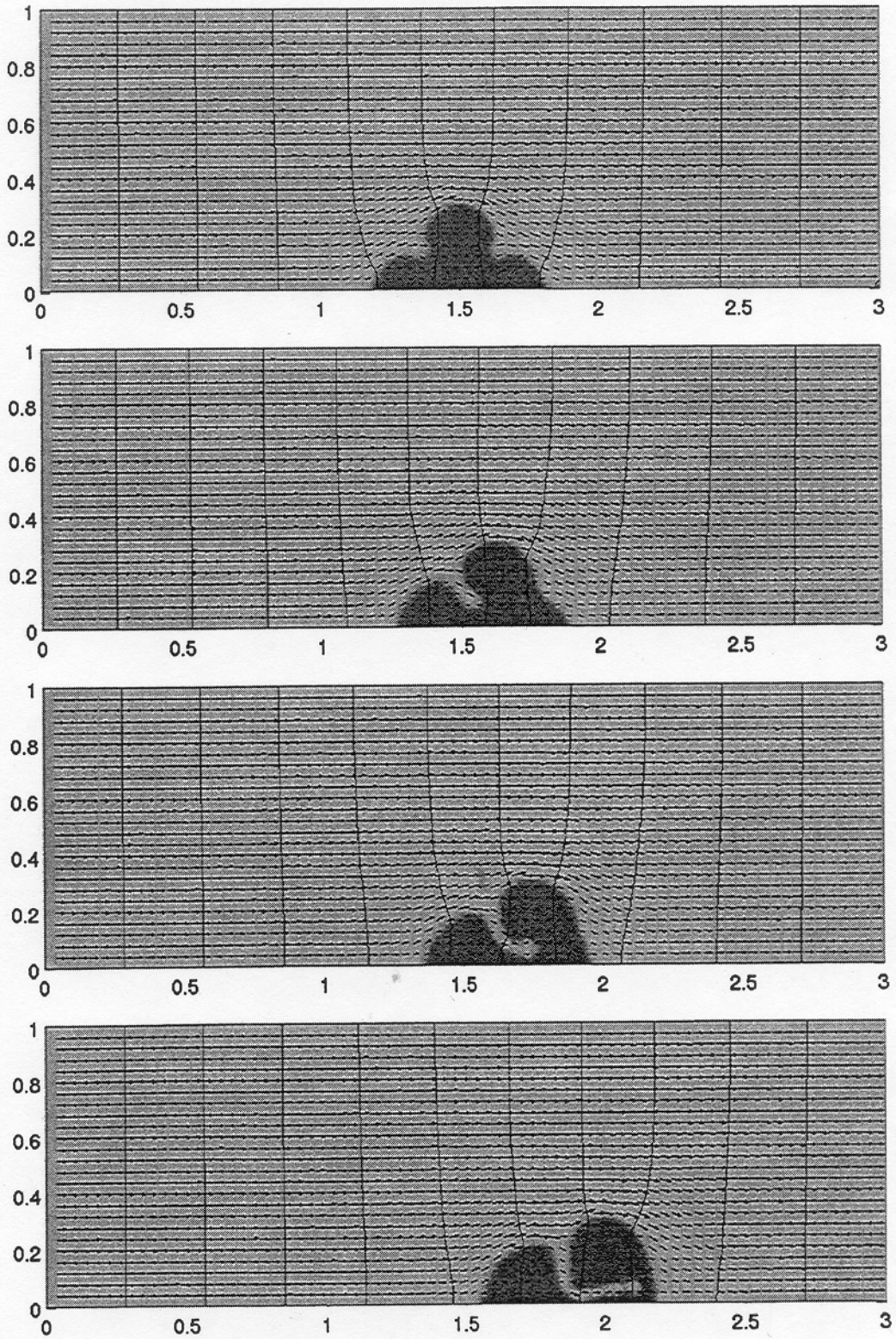

Figure 5: This figure shows dendrites for cases G–J. $1/Pr$ increases from top to bottom.

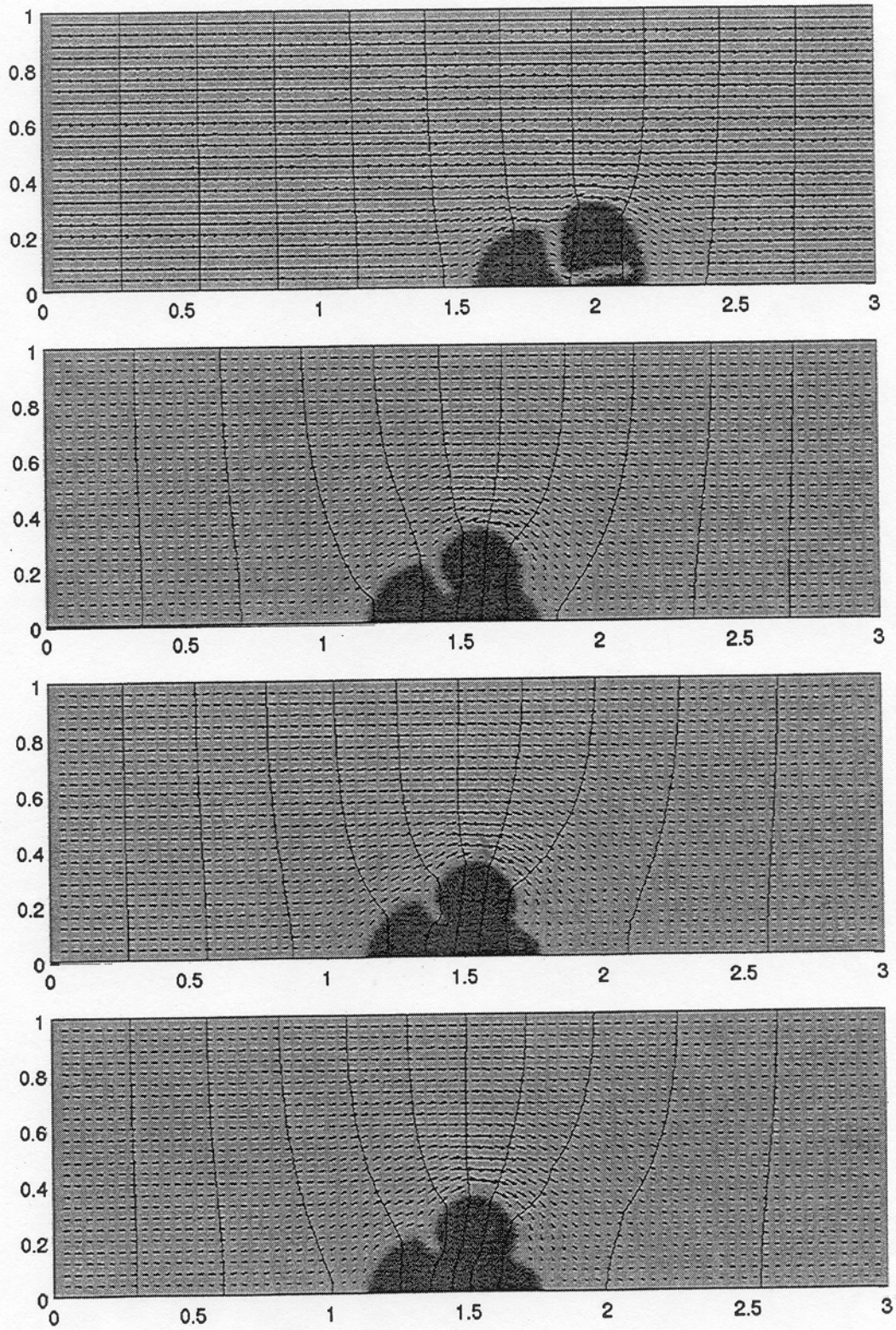

Figure 6: This figure shows dendrites for cases J–M. The value of μ is 5, 80, 160 and 320 from top to bottom.